

See discussions, stats, and author profiles for this publication at: <https://www.researchgate.net/publication/258444338>

Color rendition engineering of phosphor-converted light-emitting diodes

Article in *Optics Express* · November 2013

DOI: 10.1364/OE.21.026642 · Source: PubMed

CITATIONS

16

READS

149

6 authors, including:



Zukauskas Arturas

Vilnius University

232 PUBLICATIONS 3,794 CITATIONS

[SEE PROFILE](#)



Pranciškus Vitta

Vilnius University

78 PUBLICATIONS 927 CITATIONS

[SEE PROFILE](#)



Akvilė Zabaliūtė

Vilnius University

10 PUBLICATIONS 64 CITATIONS

[SEE PROFILE](#)



Andrius Petrulis

Vilnius University

12 PUBLICATIONS 120 CITATIONS

[SEE PROFILE](#)

Some of the authors of this publication are also working on these related projects:



H2020 NEWFOCUS COST Action [View project](#)



p-diamond Plasmonic TeraFETs [View project](#)

Color rendition engineering of phosphor-converted light-emitting diodes

Artūras Žukauskas,^{1,*} Rimantas Vaicekauskas,² Pranciškus Vitta,^{1,2} Akvilė Zabaliūtė,¹ Andrius Petrulis,¹ and Michael Shur³

¹*Institute of Applied Research, Vilnius University, Saulėtekio al. 9-III, LT-10222 Vilnius, Lithuania*

²*Department of Computer Science, Vilnius University, Didlauko g. 47, LT-08303 Vilnius, Lithuania*

³*Department of Electrical, Computer, and System Engineering, Rensselaer Polytechnic Institute, 110 8th Street, Troy, NY 12180, USA*

*arturas.zukauskas@ff.vu.lt

Abstract: We present an approach to the optimization of the trichromatic spectral power distributions (SPDs) of phosphor-converted (p-c) light-emitting diodes (LEDs) in respect of each of four different color rendition properties (high color fidelity, color saturating, color dulling, and color preference). The approach is based on selecting a model family of Eu^{2+} phosphors and finding the optimal peak wavelengths of the phosphor bands as functions of the luminous efficacy of radiation. A blue component due to either phosphor photoluminescence or InGaN electroluminescence with the peak wavelength at about 460 nm was found to be an optimal one for the high-fidelity, color-dulling, and color-preference LEDs. The high-fidelity and color-preference LEDs need red phosphors with the peak wavelength of 610–615 nm. The high-fidelity LEDs were shown to require a true green (~530 nm) phosphor component, whereas a cyan (~510 nm) component is the prerequisite of the color-saturating and color-preference LEDs. Deep-blue (~445 nm) and deep-red (~625 nm) components are required for the color-saturating LEDs. A broad yellow band similar to that of Ce^{3+} emission is to be used in the color-dulling LEDs. The SPDs of practical phosphor blends for the high-fidelity, color-saturating, and color-preference p-c LEDs are demonstrated.

©2013 Optical Society of America

OCIS codes: (160.2540) Fluorescent and luminescent materials; (160.5690) Rare-earth-doped materials; (230.3670) Light-emitting diodes; (330.1715) Color, rendering and metamerism.

References and links

1. G. Wyszecki and W. S. Stiles, *Color Science. Concepts and Methods, Quantitative Data and Formulae* (Wiley, 2000).
2. M. Shur and A. Žukauskas, "Solid-state lighting: Toward superior illumination," *Proc. IEEE* **93**(10), 1691–1703 (2005).
3. Commission Internationale de l'Éclairage, "Method of measuring and specifying colour rendering properties of light sources," *Pub. CIE* 13.3, 1995.
4. Commission Internationale de l'Éclairage, "Colour rendering of white LED sources," *Pub. CIE* 177, 2007.
5. M. S. Rea and J. P. Freyssinier-Nova, "Color rendering: A tale of two metrics," *Color Res. Appl.* **33**(3), 192–202 (2008).
6. W. Davis and Y. Ohno, "Color quality scale," *Opt. Eng.* **49**(3), 033602 (2010).
7. A. Žukauskas, R. Vaicekauskas, F. Ivanauskas, H. Vaitkevičius, P. Vitta, and M. S. Shur, "Statistical approach to color quality of solid-state lamps," *IEEE J. Sel. Top. Quantum Electron.* **15**(6), 1753–1762 (2009).
8. D. Lebedenko and R. Vaicekauskas, "Light source assessment," Vilnius University Lighting Group, <http://demo.lrg.projektas.vu.lt/lcq/en/>.
9. D. B. Judd, "A flattery index for artificial illuminants," *Illum. Eng.* **62**, 593–598 (1967).
10. W. A. Thornton, "Color-discrimination index," *J. Opt. Soc. Am.* **62**(2), 191–194 (1972).
11. W. A. Thornton, "A validation of the color-preference index," *J. Illum. Engr. Soc.* **4**, 48–52 (1974).
12. R. S. Berns, "Designing white-light LED lighting for the display of art: A feasibility study," *Color Res. Appl.* **36**(5), 324–334 (2011).
13. A. Liu, A. Tuzikas, A. Žukauskas, R. Vaicekauskas, P. Vitta, and M. Shur, "Cultural preferences to color quality of illumination of different artwork objects revealed by a color rendition engine," *IEEE Photonics J.* **5**(4), 6801010 (2013).

14. A. Žukauskas, R. Vaicekauskas, F. Ivanauskas, H. Vaitkevičius, and M. S. Shur, "Rendering a color palette by light-emitting diodes," *Appl. Phys. Lett.* **93**(2), 021109 (2008).
15. A. Žukauskas, R. Vaicekauskas, and M. S. Shur, "Solid-state lamps with optimized color saturation ability," *Opt. Express* **18**(3), 2287–2295 (2010).
16. A. Žukauskas, R. Vaicekauskas, and M. Shur, "Color-dulling solid-state sources of light," *Opt. Express* **20**(9), 9755–9762 (2012).
17. A. Žukauskas, R. Vaicekauskas, P. Vitta, A. Tuzikas, A. Petrulis, and M. Shur, "Color rendition engine," *Opt. Express* **20**(5), 5356–5367 (2012).
18. W. A. Thornton, "Luminosity and color-rendering capability of white light," *J. Opt. Soc. Am.* **61**(9), 1155–1163 (1971).
19. H. H. Haft and W. A. Thornton, "High performance fluorescent lamps," *J. Illum. Engr. Soc.* **2**, 29–35 (1972).
20. A. Žukauskas, R. Vaicekauskas, F. Ivanauskas, H. Vaitkevičius, and M. S. Shur, "Spectral optimization of phosphor-conversion light-emitting diodes for ultimate color rendering," *Appl. Phys. Lett.* **93**(5), 051115 (2008).
21. T. Jüstel, "Luminescent materials for phosphor-converted LEDs," *Luminescence*, C. Ronda, ed. (Wiley, 2008), pp. 179–190.
22. S. Ye, F. Xiao, Y. X. Pan, Y. Y. Ma, and Q. Y. Zhang, "Phosphors in phosphor-converted white light-emitting diodes: Recent advances in materials, techniques, and properties," *Mater. Sci. Eng. Rep.* **71**(1), 1–34 (2010).
23. P. F. Smet, A. B. Parmentier, and D. Poelman, "Selecting conversion phosphors for white light-emitting diodes," *J. Electrochem. Soc.* **158**(6), R37–R54 (2011).
24. R.-J. Xie, Y. Q. Li, N. Hirosaki, and H. Yamamoto, *Nitride Phosphors and Solid-State Lighting* (CRC/Taylor & Francis, 2011).
25. R. R. Jacobs, W. F. Krupke, and M. J. Weber, "Measurement of excited-state-absorption loss for Ce^{3+} in $\text{Y}_3\text{Al}_5\text{O}_{12}$ and implications for tunable $5d \rightarrow 4f$ rare-earth lasers," *Appl. Phys. Lett.* **33**(5), 410–412 (1978).
26. *Phosphor Handbook*, S. Shionoya and W. M. Yen, eds. (CRC Press, Boca Raton, 1999).
27. P. Dorenbos, "Energy of the first $4f^7 \rightarrow 4f^6 5d$ transition of Eu^{2+} in inorganic compounds," *J. Lumin.* **104**(4), 239–260 (2003).
28. W. Lehmann, "Emission spectra of (Zn,Cd)S phosphors," *J. Electrochem. Soc.* **110**(7), 754–758 (1963).
29. G. He and L. Zheng, "White-light LED clusters with high color rendering," *Opt. Lett.* **35**(17), 2955–2957 (2010).
30. M.-C. Chien and C.-H. Tien, "Multispectral mixing scheme for LED clusters with extended operational temperature window," *Opt. Express* **20**(S2 Suppl 2), A245–A254 (2012).
31. B. K. Ridley, *Quantum Processes in Semiconductors* (Oxford University Press, 2006).
32. A. Žukauskas, R. Vaicekauskas, and P. Vitta, "Optimization of solid-state lamps for photobiologically friendly mesopic lighting," *Appl. Opt.* **51**(35), 8423–8432 (2012).
33. R. Mueller-Mach, G. O. Mueller, M. R. Krames, and T. Trotter, "High-power phosphor converted light-emitting diodes based on III-nitrides," *IEEE J. Sel. Top. Quantum Electron.* **8**(2), 339–345 (2002).
34. W. M. Yen and M. J. Weber, *Inorganic Phosphors: Compositions, Preparation, and Optical Properties*, (CRC Press, 2004).
35. Y. Hu, W. Zhuang, H. Ye, S. Zhang, Y. Fang, and X. Huang, "Preparation and luminescent properties of $(\text{Ca}_{1-x}\text{Sr}_x)\text{S}:\text{Eu}^{2+}$ red-emitting phosphor for white LED," *J. Lumin.* **111**(3), 139–145 (2005).
36. X. Zhang, L. Liang, J. Zhang, and Q. Su, "Luminescence properties of $(\text{Ca}_{1-x}\text{Sr}_x)\text{Se}:\text{Eu}^{2+}$ phosphors for white LEDs application," *Mater. Lett.* **59**(7), 749–753 (2005).
37. H. Menkara, C. Summers, and B. K. Wagner, "Light-emitting device having thio-selenide fluorescent phosphor," U.S. patent No 7,109,648 (2006).
38. T. L. Barry, "Fluorescence of Eu^{2+} -activated phases of binary alkaline earth orthosilicate systems," *J. Electrochem. Soc.* **115**(11), 1181–1184 (1968).
39. H. Menkara and C. Summers, "Light emitting device having silicate fluorescent phosphor," U.S. Patent No 6,982,045 (2006).
40. S. Cheng, D. Tao, Y. Dong, and Y.-Q. Li, "Silicate-based orange phosphors," U.S. Patent No 7,655,156 (2010).
41. S. Liu, S. Cheng, and Y.-Q. Li, "Aluminum-silicate based orange-red phosphors with mixed divalent and trivalent cations," U.S. Patent No 7,648,650 (2010).
42. Y. Dong, N. Wang, S. Cheng, and Y.-Q. Li, "Aluminate based blue phosphors," U.S. Patent No 7,390,437 (2008).
43. M. Yamada, T. Naitou, K. Izuno, H. Tamaki, Y. Murazaki, M. Kameshima, and T. Mukai, "Red-enhanced white-light-emitting diode using a new red phosphor," *Jpn. J. Appl. Phys.* **42**(Part 2, No.1A/B), L20–L23 (2003).
44. Y. Q. Li, J. E. J. van Steen, J. W. H. van Krevel, G. Botty, A. C. A. Delsing, F. J. DiSalvo, G. de With, and H. T. Hintzen, "Luminescence properties of red-emitting $\text{M}_2\text{Si}_5\text{N}_8:\text{Eu}^{2+}$ ($\text{M} = \text{Ca}, \text{Sr}, \text{Ba}$) LED conversion phosphors," *J. Alloy. Comp.* **417**(1–2), 273–279 (2006).
45. R. Mueller-Mach, G. Mueller, M. R. Krames, H. A. Höpfe, F. Stadler, W. Schnick, T. Jüstel, and P. Schmidt, "Highly efficient all-nitride phosphor-converted white light-emitting diode," *Phys. Status Solidi A* **202**(9), 1727–1732 (2005).
46. K. Uheda, N. Hirosaki, Y. Yamamoto, A. Naito, T. Nakajima, and H. Yamamoto, "Luminescence properties of a red phosphor, $\text{CaAlSiN}_3:\text{Eu}^{2+}$, for white light-emitting diodes," *Electrochem. Solid-State Lett.* **9**(4), H22–H25 (2006).
47. S. Liu, D. Tao, X. Yuan, and Y.-Q. Li, "Nitride based red-emitting phosphors" U.S. Patent No 8,274,215 (2012).

48. F. Stadler, O. Oeckler, H. A. Höppe, M. H. Möller, R. Pöttgen, B. D. Mosel, P. Schmidt, V. Duppel, A. Simon, and W. Schnick, "Crystal structure, physical properties and HRTEM investigation of the new oxonitridosilicate $\text{EuSi}_2\text{O}_2\text{N}_2$," *Chemistry* **12**(26), 6984–6990 (2006).
49. V. Bachmann, C. Ronda, O. Oeckler, W. Schnick, and A. Meijerink, "Color point tuning for $(\text{Ca},\text{Sr},\text{Ba})\text{Si}_2\text{O}_2\text{N}_2:\text{Eu}^{2+}$ for white LEDs," *Chem. Mater.* **21**(2), 316–325 (2009).
50. J. W. H. van Krevel, J. W. T. van Ruten, H. Mandal, H. T. Hintzen, and R. Metselaar, "Luminescence properties of terbium-, cerium-, or europium-doped α -Sialon materials," *J. Solid State Chem.* **165**(1), 19–24 (2002).
51. R.-J. Xie, N. Hirosaki, K. Sakuma, Y. Yamamoto, and M. Mitomo, " Eu^{2+} doped $\text{Ca}-\alpha$ -SiAlON: A yellow phosphor for white light-emitting diodes," *Appl. Phys. Lett.* **84**(26), 5404–5406 (2004).
52. N. Hirosaki, R.-J. Xie, K. Kimoto, T. Sekiguchi, Y. Yamamoto, T. Suehiro, and M. Mitomo, "Characterization and properties of green-emitting β -SiAlON: Eu^{2+} powder phosphors for white light-emitting diodes," *Appl. Phys. Lett.* **86**(21), 211905 (2005).
53. X. X. Luo, W. H. Cao, and F. Sun, "The development of silicate matrix phosphors with broad excitation band for phosphor-converted white LED," *Chin. Sci. Bull.* **53**(19), 2923–2930 (2008).
54. H. A. Höppe, H. Lutz, P. Morys, W. Schnick, and A. Seilmeier, "Luminescence in Eu^{2+} -doped $\text{Ba}_2\text{Si}_2\text{N}_8$: fluorescence, thermoluminescence, and upconversion," *J. Phys. Chem. Solids* **61**(12), 2001–2006 (2000).
55. A. Žukauskas and R. Vaicekauskas, "LEDs in lighting with tailored color quality," *Int. J. High Speed Electron. Syst.* **20**(02), 287–301 (2011).
56. A. Žukauskas, R. Vaicekauskas, F. Ivanauskas, R. Gaska, and M. S. Shur, "Optimization of white polychromatic semiconductor lamps," *Appl. Phys. Lett.* **80**(2), 234–236 (2002).
57. H. F. Ivey, "Color and efficiency of luminescent light sources," *J. Opt. Soc. Am.* **53**(10), 1185–1198 (1963).
58. P. J. Bouma, "The colour reproduction of incandescent lamps and 'Philiphan' glass," *Philips' Technol. Rev.* **3**, 47–49 (1938).
59. A. Žukauskas, R. Vaicekauskas, and M. S. Shur, "Color rendition properties of solid-state lamps," *J. Phys. D Appl. Phys.* **43**(35), 354006 (2010).

1. Introduction

Present lighting technology relies on the principle of additive color mixing [1], which is implemented through composing the spectral power distribution (SPD) of white light of colored components provided by emitters having narrow and/or moderately wide bands. Such technology allows for avoiding inefficient emission at the edges of the visible spectrum, which results in improved luminous efficacy, and for engineering light sources with different correlated color temperatures (CCTs) and different color rendition characteristics.

With the development of solid-state lighting technology, which is based on either clusters of individually controlled colored light-emitting diodes (LEDs) or single-package phosphor-converted (p-c) LEDs, the application of the composite SPDs in light sources became even more versatile and artificial illumination with unsurpassable efficacy and color quality became feasible [2]. However, the diversity of SPDs of solid-state sources of light resulted in the disruption of the common metric for the assessment of the color rendition properties, the Color Rendering Index (CRI), introduced by the Commission Internationale de l'Éclairage (CIE) in 1965 [3]. In 2007, the CIE concluded that "the CIE CRI is generally not applicable to predict the colour rendering rank order of a set of light sources when white LED sources are involved in this set" [4].

The general CRI (R_a) is a measure of color fidelity for 8 test color samples and does not distinguish between the color distortions of different types. A two-metric system, which also accounts for the ability of a light source to make colors appear "vivid" and easy to distinguish (color saturating) [5], is the simplest remedy for this drawback. An approach to quantifying the ability of a light source to render object colors with high fidelity and to discriminate colors within an integral figure of merit is the Color Quality Scale (CQS) [6]. The general CQS (Q_a) is based on the disregard of the color saturating component in the color shifts of 15 test color samples. The CQS metric is supplemented by additional scales, such as color fidelity scale (Q_f), gamut area scale (Q_g), and color preference scale (Q_p). However, both the two-metric system and CQS suffer from a small number of test color samples (8 and 15, respectively), which cover a very small portion of the color space and make the assessment results dependent on the chosen sample set.

A more advanced approach to the assessment of color quality of light sources relies on analyzing color shift vectors for the entire color palette (e.g. for 1269 Munsell samples) and sorting the color test samples to several groups depending on a type of the color distortion that occurs when the reference source is replaced by that under assessment [7]. In this

statistical approach, which clearly distinguishes between different color rendition properties, the color shift vectors are computationally sorted depending on their behavior in respect of experimentally established just perceived differences of chromaticity and luminance. Then the relative numbers (percentages) of test color samples that exhibit color distortions of various types are defined as statistical color quality indices. Such indices include the Color Fidelity Index (CFI, percentage of the test samples having the color shifts smaller than perceived chromaticity differences), the Color Saturation Index (CSI, percentage of the test samples having the color shift vectors with a perceivable increase in chromatic saturation), the Color Dulling Index (CDI, percentage of the test samples having the color shift vectors with a perceivable decrease in chromatic saturation), and the Hue Distortion Index (HDI, percentage of the test samples having the color shift vectors with a perceivable distortion of hue). An on-line tool that assesses the SPDs of light sources using the statistical metric and comparing this metric with CRI and CQS is now available [8].

It is to be noted that the needs in color quality of illumination extend beyond a single need for color fidelity. In particular, it is known for years that increased color saturation can enhance the color discrimination ability and comply with visual preferences [9–11]. Even more diverse color rendition properties (ranging from increased to reduced color saturation) might be required for the illumination of complex objects, such as artwork [12,13].

The SPDs composed of distinct single-band components with the width around 30 nm typical of direct-emission LEDs have been optimized in respect of different color rendition properties measured by statistical color rendition indices CFI [14], CSI [15], and CDI [16], respectively. Recently we demonstrated a tetrachromatic LED cluster with a continuous traversing of all possible metameric SPDs including those with the highest CFI, CSI, and CDI (color rendition engine) [17]. The highest values of the statistical indices have been validated by a psychophysical experiment. The psychophysical experiment has also revealed that the appearance of familiar objects is preferred by the highest number of subjects, when a light source has an SPD with the CSI to CFI ratio between 0.3 and 3. This implies that direct-emission LED clusters can be engineered not only to improve color fidelity, which is the only one color rendition property measured by CRI, but also to optimize other color rendition properties, such as color saturating, color dulling and psychophysically validated color preference.

The color rendition engineering of SPDs composed of components typical of photoluminescence of phosphors is a more complex problem because of a large diversity of phosphor emission spectra with different numbers of bands and/or different widths of the bands. Over four decades ago, Thornton examined the trade-off between the general CRI and luminous efficacy of radiation (LER) for SPDs containing Gaussian components of different widths [18]. At that time, fluorescent lamps with the phosphor blends that render colors with both high fidelity and with high or low color discrimination had been already known [10,19]. Later, the number and width of the Gaussian components in p-c LEDs having the ultimate color fidelity (CFI = 100%) have been defined [20]. However, a general approach to the composing of practical phosphor blends for p-c LEDs that emit light with different color rendition properties has not been established so far.

In this work, the trichromatic SPDs composed of model phosphor emission bands are optimized for meeting both the requirement for high LER and different needs in color rendition (color fidelity, color saturating, color dulling, and color preference). The solutions of the optimization problem are verified by assessing the color rendition properties of the composite SPDs of p-c LEDs with the spectral components provided by commercial phosphors.

2. Color rendition engineering method

In this section, we establish the general approach to the color rendition engineering for p-c LEDs. First, we select an appropriate analytical model for their component phosphor SPDs. Second, we apply an optimization procedure for obtaining composite SPDs of trichromatic p-c LEDs with required color rendition properties.

2.1 Model phosphor spectra

Because of a large diversity of phosphors considered for the application in solid-state lighting technology [2,21–24], a general approach to color rendition engineering requires establishing model phosphor SPDs. Such component SPDs should meet the following requirements: i) the SPDs are to be related to a family of practical phosphors that have peak wavelengths within the entire visible spectrum; ii) the SPDs should be described with an appropriate accuracy by a single analytical expression containing a small number of parameters (e.g., just the peak wavelength). Once the general approaches were established for a particular model component SPD, phosphors with SPDs that considerably differ from the model ones could be considered.

In view of the above requirements, we restrict the search of model phosphors to those having a single emission band with predictable width. We do not consider phosphors that have a multiband SPD due to the spin-orbit split ground state (e.g. Ce^{3+} phosphors with $5d-4f$ transitions [25]) or due to co-doping with several types of ions. Also we do not consider phosphors emitting due to shielded $4f-4f$ transitions, which have SPDs with multiple narrow-band structure and are available only for particular spectral intervals (e.g., Eu^{3+} , Sm^{3+} , and Tb^{3+} activated phosphors [26]).

The most appropriate and versatile model phosphor components for the use in color rendition engineered SPDs are phosphors that emit due to $4f^6 5d^1-4f^7$ transitions in Eu^{2+} ions occupying similar sites within the host lattice. Such phosphors have distinct single bands with the width that has a tendency to increase (on the wavelength scale) with increasing the peak wavelength. Depending on the crystal field splitting of the $5d$ level, the peaks of the spectral bands due to Eu^{2+} emission are available within the entire visible spectrum [27].

Several approaches to the analytical approximation of phosphor emission spectra on the wavelength (λ) scale have been developed [18,20,28–30]. In this work, we approximate the SPDs of the entire family of single-band Eu^{2+} phosphors by a physically justifiable Gaussian shape on the photon energy ($h\nu$) scale [28,31]. For a SPD normalized to unit power,

$$S_{i,h\nu}(h\nu)dh\nu = 2\sqrt{\ln(2)/\pi}/W \exp\left[-4\ln(2)(h\nu - h\nu_i)^2/W^2\right]dh\nu, \quad (1)$$

where $h\nu_i$ is the peak photon energy and W is the full width at half magnitude (FWHM) measured in energy units, which generally depends on the host. On the wavelength scale, Eq. (1) converts to an asymmetrical spectrum with the width increasing with increasing peak wavelength [32]

$$S_{i,\lambda}(\lambda)d\lambda = k(\lambda/\lambda_{0i})^{-2} \exp\left[-4\ln(2)h^2c^2(\lambda^{-1} - \lambda_{0i}^{-1})^2/W^2\right]d\lambda, \quad (2)$$

where $\lambda_{0i} = c/\nu_i$ (does not exactly equal the peak position λ_i on the wavelength scale) and k is the normalization factor.

In order to develop a versatile model SPD, we attempted to apply a single value of energy FWHM to a variety of single-band Eu^{2+} phosphors described in the literature and/or patented. Figure 1 shows the wavelength FWHM of many Eu^{2+} activated phosphors plotted vs. peak wavelength. The circles, squares, diamonds, upward and downward triangles, and stars show the data for chalcogenides (sulfides [33–35] and selenides [36] of alkaline earth metals as well as thiochalcogenides [33,37]), silicates [38–41], aluminates [34,42], nitridosilicates [43–47], oxonitridosilicates (SiONs) [45,48,49], and oxonitridoaluminosilicates (SiAlONs) [50–52], respectively. Since some Eu^{2+} phosphors are known to exhibit a dual structure of the emission band due to the presence of the activator at different sites of the host lattice (e.g. in orthosilicates and pentasilicates [53] and nitridosilicate phosphors [54]), we sorted these data in respect to the appropriateness of the single-band model. The solid points in Fig. 1 show the data for phosphor bands that can be approximated by Eq. (2) with the coefficient of determination (R^2) above 0.99. The data for phosphor bands that were approximated with $R^2 < 0.99$ are presented by open points.

The solid line in Fig. 1 shows the wavelength FWHM for SPDs described by Eq. (2) for the constant energy width, W , of 0.27 eV ($\sim 2200 \text{ cm}^{-1}$). This model FWHM monotonously increases from 44 nm to 93 nm, when the peak wavelength varies from 450 nm to 650 nm. The FWHM of most Eu^{2+} phosphors that have distinct single-band SPDs ($R^2 > 0.99$; solid points) deviate from the model value by less than 20 nm. Generally, the chalcogenide phosphors have FWHMs that are somewhat smaller than the model ones due to small phonon frequencies [27]; also, the SPDs of these phosphors are well fit to the single-band model. Most aluminates, silicates and nitrides have FWHMs that are almost equal or somewhat larger than those suggested by the model; many of them have SPDs that deviate from Eq. (2).

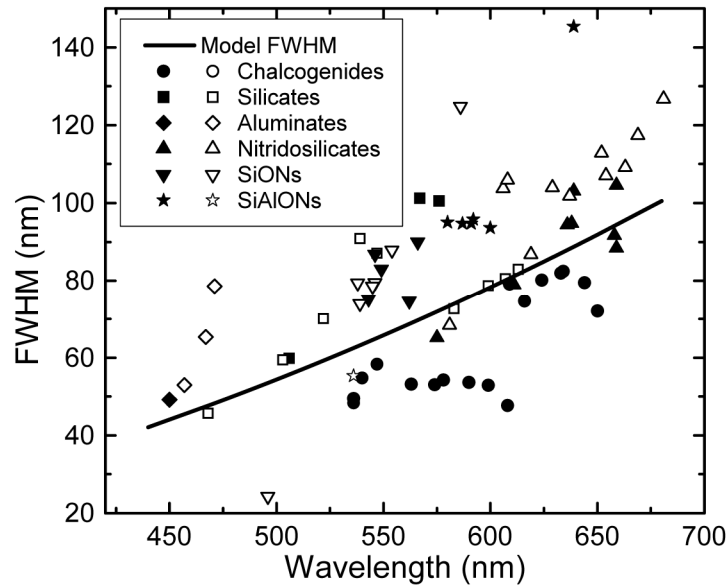


Fig. 1. Wavelength FWHM of Eu^{2+} activated phosphors vs. peak wavelength. Circles, chalcogenides [33–37]; squares, silicates [38–41]; diamonds, aluminates [34,42]; upward triangles, nitridosilicates [43–47]; downward triangles, SiONs [45,48,49]; and stars, SiAlONs [50–52], respectively. The solid and open points show data for phosphor bands that can be approximated by a single-band model with $R^2 > 0.99$ and $R^2 < 0.99$, respectively.

At the peak wavelength of 450 nm, the model phosphor FWHM (44 nm) is comparable to that of the emission bands of blue InGaN LEDs (18–25 nm). Such blue emission is used as a short-wavelength component and for the photoexcitation of phosphors in the white LEDs with partial conversion. Substituting the blue phosphor components used in the SPDs of the white LEDs with complete conversion by somewhat narrower InGaN components might influence the color rendition indices as discussed below.

Figure 2 shows examples of the SPDs of Eu^{2+} phosphors (solid lines) compared with the model SPDs (dashed lines) of the same bandwidth. The blue phosphor is $\text{Ba}_{0.6}\text{Eu}_{0.4}\text{MgAl}_5\text{O}_{17}$ (BAM [42]) with the peak wavelength of 450 nm and FWHM of 49 nm, the cyan phosphor is $\text{Ba}_2\text{SiO}_4:\text{Eu}^{2+}$ [39] (506 nm peak wavelength, 60 nm FWHM), the yellow phosphor is $\text{EuSi}_2\text{O}_2\text{N}_2$ [48] (586 nm peak wavelength, 125 nm FWHM), and the red phosphor is $\text{SrS}:\text{Eu}^{2+}$ [33] (616 nm peak wavelength, 75 nm FWHM). The SPDs of the blue, cyan, and red phosphors are reasonably fit by Eq. (2) with $R^2 > 0.99$ and deviate in the peak wavelength from the model spectra by less than 3 nm, which is the uncertainty of our single-band model. The SPD of the yellow phosphor poorly fits the single-band model with $R^2 = 0.978$ and with the peak wavelength deviation of about 10 nm.

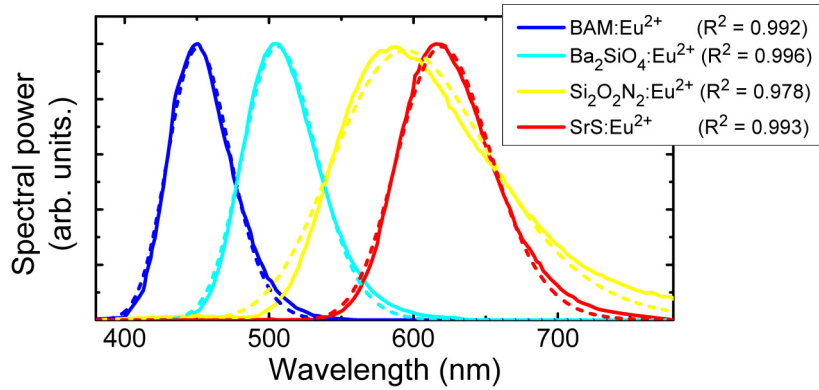


Fig. 2. Examples of the SPDs of Eu^{2+} phosphors (solid lines) and fits to model single-band SPDs with the same width (dashed lines). Blue phosphor, BAM (after [42]); cyan phosphor, $\text{Ba}_2\text{SiO}_4:\text{Eu}^{2+}$ (after [39]); yellow phosphor, $\text{EuSi}_2\text{O}_2\text{N}_2$ (after [48]); and red phosphor, $\text{SrS}:\text{Eu}^{2+}$ (after [33]).

2.2 Optimization procedure

Our optimization procedure for obtaining composite SPDs of p-c LEDs with required color rendition properties is as follows. Using the equations of color mixing [55], three different spectral components described by Eq. (2) are combined into a trichromatic blend with the partial radiant fluxes selected in such a way that the resultant chromaticity coordinates are equal to those of the blackbody illuminant with the CCTs of 3000 K or 4500 K or of the daylight phase illuminant with the CCT of 6500 K. The optimal composite SPDs are found for each CCT as functions of LER by maximizing an objective function for each of four color rendition properties under consideration.

For high color fidelity blends, the objective function to be maximized is

$$F_{\text{CCT,LER}}(\lambda_1, \lambda_2, \lambda_3, p_1, p_2, p_3) = \text{CFI}, \quad (3)$$

where λ_1, λ_2 , and λ_3 and p_1, p_2 , and p_3 are the peak wavelengths and partial radiant fluxes of the three model phosphors.

For color-saturating blends, the objective function to be maximized is

$$F_{\text{CCT,LER}}(\lambda_1, \lambda_2, \lambda_3, p_1, p_2, p_3) = \text{CSI}|_{\text{HDI} \leq 50\%}. \quad (4)$$

Here and below, the objective functions for non-fidelity blends are subjected to a constraint $\text{HDI} \leq 50\%$ in order to avoid solutions with a high hue distortion.

For color-dulling blends, the objective function to be maximized is

$$F_{\text{CCT,LER}}(\lambda_1, \lambda_2, \lambda_3, p_1, p_2, p_3) = \text{CDI}|_{\text{HDI} \leq 50\%}. \quad (5)$$

For color-preference blends, the objective function to be maximized is

$$F_{\text{CCT,LER}}(\lambda_1, \lambda_2, \lambda_3, p_1, p_2, p_3) = \text{CSI/CFI}|_{\substack{\text{HDI} \leq 50\% \\ \text{CDI} \leq 10\%}}. \quad (6)$$

Here the objective function is subjected to an additional constraint $\text{CDI} \leq 10\%$ in order to avoid solutions with both CSI and CFI low.

In all cases, the six variables of the objective function must satisfy three equations following from the principle of additive color mixing [55]. Therefore, the objective functions were maximized within the optimization domain, which is the parametric space with 3 degrees of freedom. Once a CCT and LER were selected, the maximization of the objective

function was performed using a computer routine that performs stochastic searching on a three-dimensional parametric surface [56].

3. Results and discussion

In this section, we present the results of the optimization of the trichromatic SPDs for the high color fidelity, color saturating, color dulling, and color-preference blends of the model Eu^{2+} phosphors. The optimization was performed using the objective functions described above. For each type of the blend optimized in respect of a statistical color rendition index or a combination of color rendition indexes, the peak wavelengths of the three phosphors are displayed and other statistical indices and the general CRI and relevant CQS scales are estimated. Finally, the data on peak wavelengths obtained from the optimization of the model SPDs are used for the selection of commercially available Eu^{2+} phosphors and for the generation of the SPD examples for high color fidelity, color-saturating, and color-preference blends. The component phosphor spectra are used without accounting for a possible effect of a partial reabsorption of light emitted by shorter-wavelength phosphors in longer-wavelength phosphors.

3.1 High-fidelity blends

Figures 3(a), 3(b), and 3(c) show the dependences of maximized CFI (pink circles) on LER for the trichromatic blends of model Eu^{2+} phosphors at CCTs of 3000 K, 4500 K, and 6500 K, respectively. These dependences establish the trade-off between CFI and LER (the Pareto frontier). Extremely high values of CFI (over 90%) can be attained at lower LERs, whereas the color fidelity as a dominant property of the blends ($\text{CFI} > 50\%$) can be retained up to the LERs of 315-350 lm/W, depending on the CCT. Generally, the optimal blends with lower CCTs have higher LERs for the comparable values of CFI. Also shown in Figs. 3(a), 3(b), and 3(c) are common color fidelity indices (R_a and CQS Q_f), as well as the indices quantifying distortions of chroma (CSI and CDI). The variations of R_a and CQS Q_f are in line with the CFI, although the latter is a more sensitive indicator of color fidelity. In the entire range of LERs, the optimal blends show almost no color saturating ability (the CSI is marginal); whereas with increasing LER and reducing CFI, a noticeable fraction of colors are losing chroma (the CDI gradually approaches CFI).

Figures 3(d), 3(e), and 3(f) show the corresponding peak wavelengths of the three model phosphors for the optimized high color fidelity blends. The general feature of all the SPDs is an almost equal distance between the adjacent peaks of about 80 nm and synchronous shifting to shorter wavelengths with increasing LER and decreasing CFI. Also, phosphors with longer peak wavelengths are to be used in the optimal blends with comparable CFIs for lower CCTs. A reasonable trade-off between color fidelity and LER is obtained for phosphor peak wavelengths of about 460 nm, 530 nm, and 615 nm. Due to the asymmetry and different wavelength widths of the practical Eu^{2+} phosphor bands, these peak wavelengths are shorter (especially the longest one) than those obtained for high-fidelity SPDs with symmetrical and equal-width bands (470 nm, 560 nm, and 660 nm; all 80 nm wide [20]). Another important result is that the red-green-blue (RGB) p-c LEDs, which have wide-band spectral components, yield high color fidelity, in contrast to the direct-emission (narrow-band) RGB LED clusters, which are essentially color saturating [15].

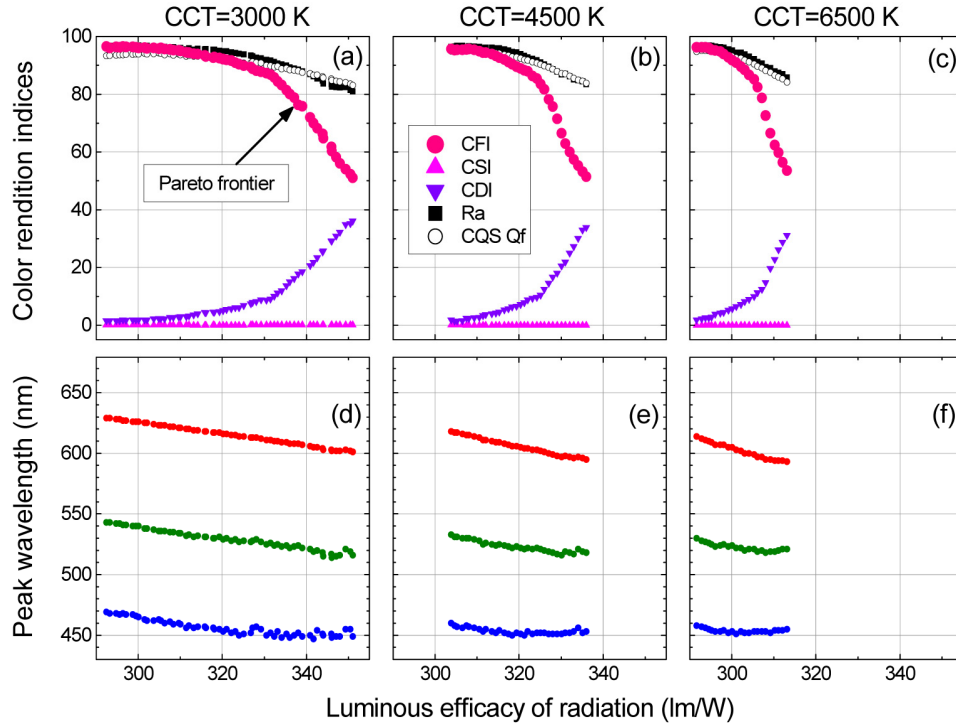


Fig. 3. (a), (b), and (c) Maximized statistical color fidelity index (pink circles) vs. LER for the trichromatic blends of model Eu^{2+} phosphors at CCTs of 3000 K, 4500 K, and 6500 K, respectively. Also shown are CSI (magenta triangles), CDI (violet triangles), R_a (black squares), and CQS Q_f (open circles). (d), (e), and (f) Corresponding peak wavelengths of the three model phosphors.

Figures 4(a), 4(b), and 4(c) show examples of the SPDs of the high color fidelity blends of commercial phosphors for the three CCT values, respectively. All SPDs are composed of the same blue BAM (Intematix B101C-2; 446 nm peak wavelength, 45 nm FWHM), green silicate (Intematix EG3264; 528 nm peak wavelength, 71 nm FWHM), and red nitride (PhosphorTech HTR620; 617 nm peak wavelength, 83 nm FWHM) phosphors. The SPDs have CFIs of 88%, 73%, and 56% and LERs of 307 lm/W, 300 lm/W, and 289 lm/W for CCTs of 3000 K, 4500 K, and 6500 K, respectively. For the CCT of 3000 K, the SPD parameters are close to the optimal ones [Fig. 3(a)]. For higher CCTs, the values of CFI and LER are somewhat lower than those on the Pareto frontier in favor of CDI due to the longer than required peak wavelengths of the red and green phosphors.

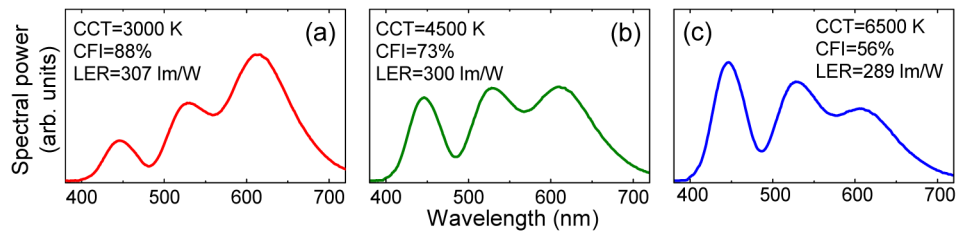


Fig. 4. (a), (b), and (c) Examples of high color fidelity trichromatic SPDs composed of commercial blue BAM (Intematix B101C-2), green silicate (Intematix EG3264), and red nitride (PhosphorTech HTR620) Eu^{2+} phosphors for CCTs of 3000 K, 4500 K, and 6500 K, respectively. The values of CFI and LER are indicated.

When the blue phosphor component is replaced with a narrower one (24 nm wide, not shown) provided by InGaN electroluminescence and having the same peak wavelength, the CFI decreases by 3-10%, whereas the LER increases by 3-9 lm/W (depending on the CCT). The limiting radiant efficiency of such LEDs (with CFI of ~80%) accounting for the Stokes shift [57] is about 80% assuming the radiant efficiency of the blue emitter and the quantum efficiency of the phosphors of 100%. This shows that high-fidelity p-c LEDs with the partial conversion of InGaN emission in green and red phosphors are feasible with a luminous efficacy of about 260 lm/W.

When the red component is replaced by a narrow band, such as multiple-line emission, typical of Eu^{3+} phosphors, high color fidelity becomes difficult to achieve,

3.2 Color-saturating blends

Figures 5(a), 5(b), and 5(c) show the dependence of maximized CSI (magenta triangles) on LER for the trichromatic blends of the model Eu^{2+} phosphors for CCTs of 3000 K, 4500 K, and 6500 K, respectively. Again, a well-established Pareto frontier shows that the CSI and LER are in negative trade-off. High values of CSI (over 60%) can be attained at lower LERs, whereas the domination of the color saturating ability ($\text{CSI} > 50\%$) can be retained up to the LERs of 270-280 lm/W, depending on the CCT. The optimal blends with lower CCTs have higher LERs for the comparable values of CSI; also, somewhat higher values of CSI can be attained at lower CCTs. The general CRI of the color saturating blends is always below 80 and shows a tendency to increase with decreasing CSI. The CQS gamut area scale Q_g is above 80 and varies almost in the same way as CSI. In the entire range of LERs, the optimal blends show a low color dulling ability ($\text{CDI} < 10\%$) and low color fidelity ($\text{CFI} < 20\%$). These two indices show some increase with reduced CSI.

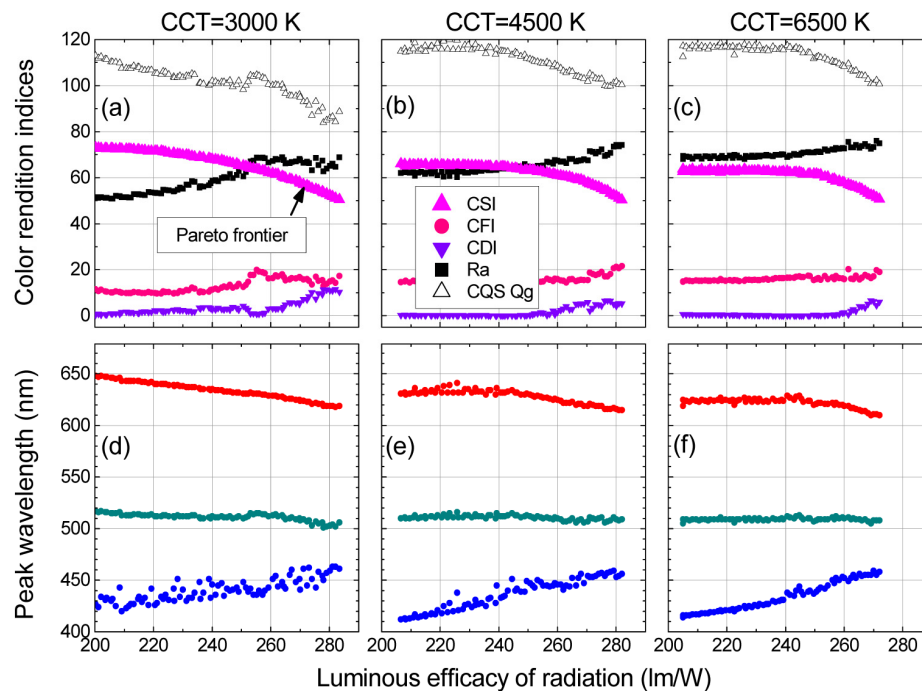


Fig. 5. (a), (b), and (c) Maximized statistical color saturating index (magenta triangles) vs. LER for the trichromatic blends of model Eu^{2+} phosphors at CCTs of 3000 K, 4500 K, and 6500 K, respectively. Also shown are CFI (pink circles), CDI (violet triangles), R_a (black squares), and CQS Q_g (open triangles). (d), (e), and (f) Corresponding peak wavelengths of the three model phosphors.

Figures 5(d), 5(e), and 5(f) show the corresponding peak wavelengths of the three model phosphors for the optimized color saturating blends. In comparison to the high-fidelity blends (Fig. 3), the optimal color-saturating blends have the red component shifted to longer wavelengths, whereas the green and blue components are shifted to shorter wavelengths (actually, the middle component should be more accurately named as cyan). The crucial requirement for the color saturating blends is an asymmetry in the distribution of the components with a large gap in the yellow-green region of the spectrum, where the spectral power of a light source is to be reduced for improved color discrimination [15,58]. With increasing LER and decreasing CSI, the red and blue peaks shift toward the center of the visible spectrum, whereas the cyan peak persists at about 510 nm. Also in the optimal blends with comparable CSIs, phosphors with longer peak wavelengths are to be used for lower CCTs. Due to the asymmetry of the Eu^{2+} phosphor bands, only the red-cyan-blue (RCB) color saturating p-c LEDs are feasible. This is different from the clusters of direct-emission LEDs, where the color saturating property is a characteristic of both the RCB and RGB blends [15].

Figures 6(a), 6(b), and 6(c) show examples of the SPDs of the color-saturating blends of commercial phosphors for the three CCT values, respectively. All SPDs are composed of the same blue BAM (Intematix B101C-2; 446 nm peak wavelength, 45 nm FWHM), cyan silicate (Intematix G1758; 507 nm peak wavelength, 59 nm FWHM), and deep red nitride (Intematix ER6436; 625 nm peak wavelength, 87 nm FWHM) Eu^{2+} phosphors. The SPDs have CSIs of 59%, 61%, and 62% and LERs of 255 lm/W, 249 lm/W, and 241 lm/W, for CCTs of 3000 K, 4500 K, and 6500 K, respectively. All these parameters are close to those at the Pareto frontier [Figs. 5(a)-5(c)].

When the blue phosphor component is replaced with a narrower one (24 nm wide, not shown) provided by the electroluminescence of InGaN and having the same peak wavelength, the CSI and LER remain almost unchanged for all CCTs. The limiting radiant efficiency of such LEDs (with CSI of ~60%) accounting for the Stokes shift [57] is 82% for all considered CCTs assuming the radiant efficiency of the blue emitter and the quantum efficiency of the phosphors of 100%. This enables the development of the color-saturating p-c LEDs with the partial conversion of InGaN emission in cyan and red phosphors with a limiting luminous efficacy of about 230 lm/W.

When the red component is replaced by a narrow band one, such as multiple-line emission typical of Eu^{3+} phosphors, both the color saturating ability and LER can be increased.

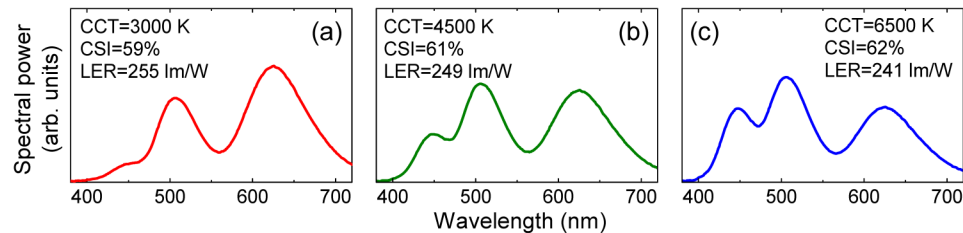


Fig. 6. (a), (b), and (c) Examples of color-saturating trichromatic SPDs composed of commercial blue BAM (Intematix B101C-2), cyan silicate (Intematix EG1758), and deep red nitride (Intematix ER6436) Eu^{2+} phosphors for CCTs of 3000 K, 4500 K, and 6500 K, respectively. The values of CSI and LER are indicated.

3.3 Color-dulling blends

Figures 7(a), 7(b), and 7(c) show the dependence of the maximized CDI (violet triangles) on LER for the trichromatic blends of model Eu^{2+} phosphors at CCTs of 3000 K, 4500 K, and 6500 K, respectively. Here, the Pareto frontier is almost flat, indicating that the color-dulling blends with the highest LER are the most appropriate. The maximized CDI has values of 73%, 64%, and 62% for the peak LERs of 410 lm/W, 370 lm/W, and 335 lm/W at the three CCTs, respectively. The general CRI of the optimal color dulling blends is below 70, similarly to color-saturating blends (this reveals the ambiguity of R_a in respect of the opposite

dominating chroma distortion type mentioned above and discussed in [17]) and shows a tendency to decrease with increasing LER and CCT. The CQS gamut area scale Q_g is below 80. In the entire range of LERs, the optimal blends increase chroma of almost no colors (CSI $\approx 0\%$) and have a low color fidelity (CFI $< 20\%$).

Figures 7(d), 7(e), and 7(f) show the corresponding peak wavelengths of the three model phosphors in the optimized color dulling blends. The blue component stays at about 460 nm within the entire range of LERs. The other two components tend to coalesce in the yellow region of the spectrum. At the highest LERs relating to the most appropriate blends, the long-wavelength component approaches to and overlaps with the middle (yellow-green) one. Similar results were obtained for the color-dulling SPDs composed of symmetrical narrow blue and wide yellow bands [16]. Such an alignment of the spectral components is typical of common white InGaN/Y₃Al₅O₁₂:Ce³⁺ LED with a narrow-band blue and wide-band yellow emissions (the latter is due to the spectral overlap of two spin-orbit split emission bands of Ce³⁺). A typical daylight p-c LED (CCT = 6042 K) has a CDI of 53%, CFI of 17%, CSI of 4%, and LER of 325 lm/W [59], which are the values close to those of the optimized color-dulling blend [Fig. 7(c)]. The limiting radiant efficiency of dichromatic color-dulling LEDs (with CDI of ~ 60 -70%) with partial conversion in Eu²⁺-based phosphors accounting for the Stokes shift [57] is 83-89% (depending on the CCT) assuming the radiant efficiency of the blue emitter and the quantum efficiency of the phosphors of 100%. This corresponds to the limiting luminous efficacies in the range of 300-340 lm/W depending on the CCT. However since the use of broad-band yellow Ce³⁺-based phosphors is a well-established approach, the application of more sophisticated Eu²⁺-based phosphor blends in color-dulling LEDs is of doubtful value (for this reason, we present no SPDs for commercial phosphors).

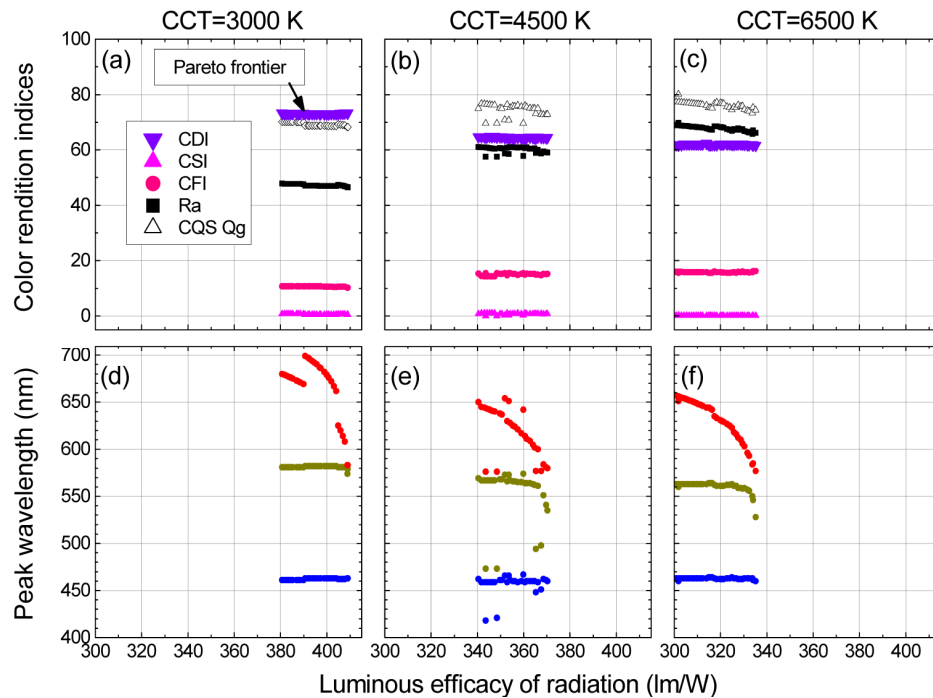


Fig. 7. (a), (b), and (c) Maximized statistical color dulling index (violet triangles) vs. LER for the trichromatic blends of model Eu²⁺ phosphors at CCTs of 3000 K, 4500 K, and 6500 K, respectively. Also shown are CFI (pink circles), CSI (magenta triangles), R_a (black squares), and CQS Q_g (open triangles). (d), (e), and (f) Corresponding peak wavelengths of the three model phosphors.

3.4 Color-preference blends

Figures 8(a), 8(b), and 8(c) show the dependence of the maximized CSI to CFI ratio (crosses) versus LER for the trichromatic blends of the model Eu^{2+} phosphors at CCTs of 3000 K, 4500 K, and 6500 K, respectively. The chosen range of the CSI/CFI ratio (0.3-3) corresponds to the highest preference of selecting tetrachromatic RAGB blends using a tunable color-rendition engine for an illuminated scene containing common objects [17]. The dependences can be considered in terms of the Pareto frontiers indicating that higher CSI/CFI ratios are attained at the expense of LER. With increasing CCT, these frontiers shift to lower LERs. With increasing the CSI/CFI ratio, CSI increases and CFI decreases, both having values of about 30% at CSI/CFI = 1. The general CRI of the color preference blends is around 85 for CSI/CFI = 0.3 and decreases to about 70 at the CSI/CFI ratio of 3. The same behavior is characteristic of the color preference scale Q_f , which has been introduced into CQS without a proper psychophysical validation. (Therefore, the CQS Q_f shows no maximum at a CSI/CFI ratio of about unity, where the highest subjective preference has been observed [17].) The color-preference blends dull very few colors (CDI < 10%).

Figures 8(d), 8(e), and 8(f) show the corresponding peak wavelengths of the three model phosphors for the optimized color-preference blends. These peak wavelength positions have similarities with both those of high color fidelity blends and color-saturating blends. The middle peak resides at about 510 nm, similarly to the color saturating blends (Fig. 5), whereas the outer blue and red peaks at about 460 nm and 610 nm are similar to those in the high-fidelity blends (Fig. 3). Also, the gap between the red and cyan components is larger than that between the cyan and blue components. With increasing LER and decreasing the CSI/CFI ratio, the red peak shifts toward shorter wavelengths, the cyan peak exhibits a small shift to longer wavelengths, and the blue peak remains at approximately the same wavelength. An increased CCT results in some shrinking of the entire spectrum.

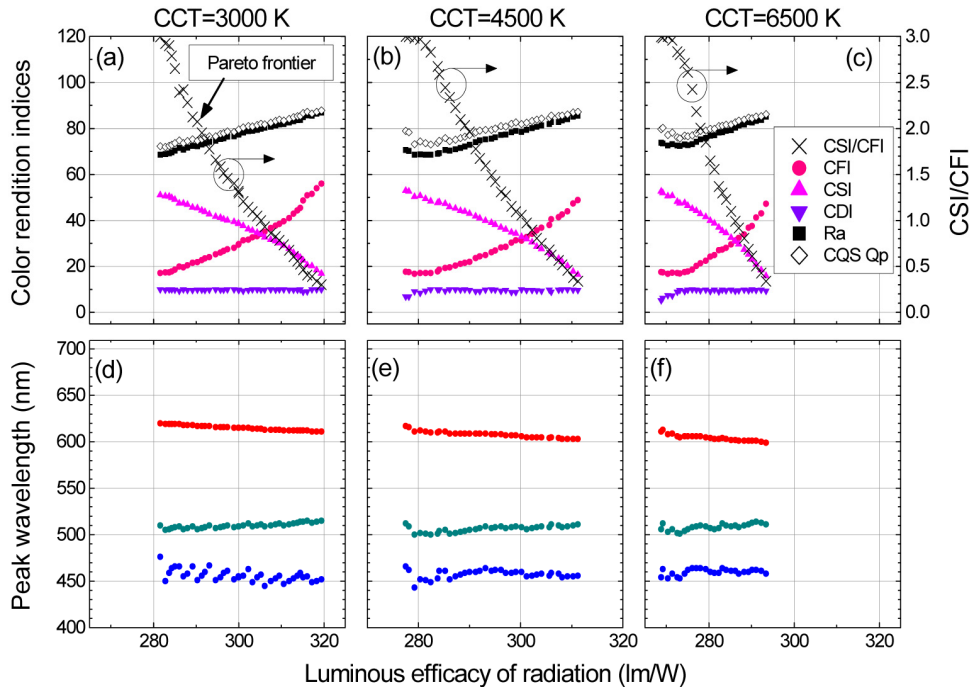


Fig. 8. (a), (b), and (c) Maximized ratio of the statistical color saturating index and color-fidelity index (crosses) vs. LER for the trichromatic blends of model Eu^{2+} phosphors at CCTs of 3000 K, 4500 K, and 6500 K, respectively. Also shown are CFI (pink circles), CSI (magenta triangles), CDI (violet triangles), R_a (black squares), and CQS Q_p (open diamonds). (d), (e), and (f) Corresponding peak wavelengths of the three model phosphors.

Figures 9(a), 9(b), and 9(c) show examples of the SPDs of the color-preference blends of commercial phosphors for the three CCT values, respectively. All SPDs are composed of the same blue BAM (Intematix B101C-2; 446 nm peak wavelength, 45 nm FWHM), cyan silicate (Intematix G1758; 507 nm peak wavelength, 59 nm FWHM), and red-orange silicate (Intematix O6040; 606 nm peak wavelength, 81 nm FWHM) Eu^{2+} phosphors. The ratios of CSI to CFI are 0.60, 0.97, and 1.22 and the LERs are 304 lm/W, 286 lm/W, and 268 lm/W, for CCTs of 3000 K, 4500 K, and 6500 K, respectively. The CSI/CFI ratios fall within the preference range of 0.3 to 3, whereas the LERs are somewhat smaller than the optimal ones [see Figs. 8(a)-8(c)] due to the lack of the exact match of the phosphor peak wavelengths with those predicted.

When the blue phosphor component is replaced by a narrower one corresponding to the InGaN emission (24 nm wide, not shown) the CSI to CFI ratio decreases by just 0.03 to 0.14 and LER increases by 2-6 lm/W depending on the CCT. The limiting radiant efficiency of such LEDs (with CSI/CFI of ~ 1) accounting for the Stokes shift [57] is 83% for all considered CCTs assuming the radiant efficiency of the blue emitter and the quantum efficiency of the phosphors of 100%. This implies that our optimization data can be used for designing phosphor blends for the color-preference p-c LEDs with partial conversion with a limiting luminous efficacy of about 250 lm/W.

A narrow-band red component due to multiple-line emission typical of Eu^{3+} phosphors is expected to increase CSI and decrease CFI; therefore, the ratio of those would increase accompanied by an increase in LER.

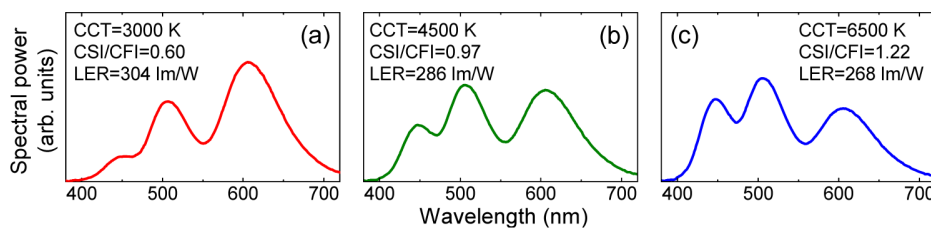


Fig. 9. (a), (b), and (c) Examples of color-preference trichromatic SPDs composed of commercial blue BAM (Intematix B101C-2), cyan silicate (Intematix EG1758), and red-orange silicate (Intematix O6040) Eu^{2+} phosphors for CCTs of 3000 K, 4500 K, and 6500 K, respectively. The values of CSI/CFI and LER are indicated.

5. Summary

We demonstrated an approach to the color rendition engineering of p-c LEDs based on maximizing LER and each of four different color rendition properties (color fidelity, color saturating, color dulling, and color preference). The optimal SPDs of the LEDs were composed of model phosphor emission bands with the shape typical of the common Eu^{2+} phosphors. The optimization results yield examples of the SPDs of the high color fidelity, color-saturating, and color-preference LEDs using commercial phosphors. The optimal color-dulling LEDs were found to have SPDs very similar to those of the commercial $\text{InGaN/Y}_3\text{Al}_5\text{O}_{12}:\text{Ce}^{3+}$ LEDs.

Table 1 displays the proposed approximate peak wavelengths of Eu^{2+} activated phosphors required for the trichromatic p-c LEDs with different color rendition properties. Blue phosphors with a peak wavelength of about 460 nm are required for the high-fidelity, color-dulling and color-preference p-c LEDs with complete conversion. For the color-saturating LEDs, deeper-blue phosphors (~ 445 nm) are preferable. In the p-c LEDs with partial conversion, the blue phosphor component can be replaced by a narrower band provided by InGaN electroluminescence without a big impact on the color rendition properties. The high-fidelity p-c LEDs require a true green component (~ 530 nm), whereas in the color-saturating and color preference LEDs, this component has to be replaced by the cyan one (~ 510 nm).

The color-dulling LEDs need a broad band in the yellow spectral region with a peak wavelength in the range around 580 nm. The optimal peak wavelength of the red component of the high-fidelity and color-preference p-c LEDs has to be chosen in the range of 610-615 nm. A deeper-red component (620-630 nm) is required for the color-saturating LEDs.

Table 1. Proposed approximate peak wavelengths of Eu^{2+} activated phosphors required for the trichromatic phosphor converted LEDs with different color rendition properties.

Color rendition property	Deep blue	Blue	Cyan	Green	Yellow	Red	Deep red
High fidelity		460		530		615	
Color saturating	445		510				625
Color dulling		460		~580			
Color preference		460	510			610	

Acknowledgments

The work at VU was partially funded by a grant from the Research Council of Lithuania. (No. MIP-098/2012). P.V. acknowledges a postdoctoral fellowship funded by the European Union Structural Funds project “Postdoctoral Fellowship Implementation in Lithuania.” The work at RPI was supported primarily by the Engineering Research Centers Program (ERC) of the National Science Foundation under NSF Cooperative Agreement No. EEC-0812056 and in part by New York State under NYSTAR contract C090145.